Accepted Article

Title: Further studies on how the nature of zeolite cavities that are bounded by small pores influences the conversion of methanol to light olefins

Authors: Jong Hun Kang, Raimund Walter, Dan Xie, Tracy Davis, Cong-Yan Chen, Mark Edward Davis, and Stacey Zones

Further Studies on How the Nature of Zeolite Cavities That are Bounded by Small Pores

Influences the Conversion of Methanol to Light Olefins

by

Jong Hun Kang[#], Raimund Walter[#], Dan Xie, Tracy Davis, Cong-Yan Chen, Mark E. Davis[#,*] and Stacey I. Zones*

[#]Chemical Engineering, California Institute of Technology, Pasadena, California 91125, United States

Chevron Energy Technology Company, 100 Chevron Way, Richmond, California 94802, United States

ABSTRACT

A series of small pore zeolites are synthesized and investigated as catalysts for the methanol-to-olefins (MTO) reaction. Small pore zeolites SSZ-13, SSZ-16, SSZ-27, SSZ-28, SSZ-52, SSZ-98, SSZ-99, SSZ-104, SSZ-105 and an ITQ-3-type material are synthesized, and the results from their use as catalytic materials in the MTO reaction compared to those obtained from SAPO-34. The production of propane that tends to correlate with catalytic material lifetime (higher initial propane yields lead to shorter lifetimes) declines with increasing Si/Al (as has been observed previously for SSZ-13), and a larger cage dimension leads to higher propane yields at a fixed Si/Al. Data from these materials and others reported previously, e.g., SSZ-39 and Rho, that were tested at the same reaction conditions, revealed four different patterns of light olefin selectivities: (i) ethylene greater than propylene with low butene, e.g., SSZ-17, SSZ-98, SSZ-105, (ii) ethylene equal to propylene and low butene, e.g., SAPO-34, SSZ-13, SSZ-16, SSZ-27, SSZ-52, SSZ-99, SSZ-104, (iii) propylene greater than ethylene with butene similar to ethylene, e.g., SSZ-28, SSZ-39, and (iv) ethylene equal to propylene equal to butene, e.g., Rho. No clear relationships between zeolite cage architecture and light olefin selectivity emerged from this investigation, although several trends are presented as suggestions for further study.

INTRODUCTION

The use of small pore zeolites as catalysts for the conversion of methanol-to-olefins (MTO) has been the topic of numerous studies. However, there remains opportunities to investigate further this reaction system because: (i) it is having an increased commercial significance, and (ii) it involves mechanisms that are non-traditional for zeolite catalysts, i.e., they do not utilize traditional shape-selectivity as the origin of product distribution, and the structure-property relationships are unclear at this time. The MTO reaction, while investigated for decades, is now a commercial development as part of the portfolio of coal-to-olefins in China [1]. Research carried out in China for a number of years has led to their use of a small pore molecular sieve, a silicoaluminophosphate material, SAPO-34 [1-3], that possesses a CHA topology (three letter codes for molecular sieve topologies, and details of each

topology can be found at the International Zeolite Association Database of Zeolite Structures). By replacing some of the P atoms in an aluminophosphate with Si atoms, Bronsted acid sites are formed, and are used to catalyze the MTO reaction [1, 4, 5]. SAPO-34 is one of a few SAPO materials studied for this application. In contrast, there is an increasing number of aluminosilicate, small pore zeolites that have been reported and investigated as catalysts [5-7]. The development of this type of zeolite material has been spurred by the finding that they make outstanding catalysts for the emission-control application for the conversion of NO_x gases into nitrogen and oxygen, when properly exchanged with copper ions [8, 9]. This application has been commercialized by Ford Motors [10].

Structural features of the catalysts for the MTO and $deNO_x$ reactions are known to significantly contribute to their success. For both reactions, the small pores are important. For the MTO reaction, there appears to be a requirement of a cage with sufficient size to accommodate and confine aromatic intermediates in order for the reaction to proceed with high selectivity to light olefins [1, 11], and the product distributions can depend on the cage geometries. [7, 12, 13] Additionally, the Si/Al ratios of the zeolite catalysts can be critical to their performance, as Bronsted acid sites that are in close proximity to one another (at lower Si/Al ratios and quantified by divalent cation exchange capacity) have been shown to be detrimental to the lifetimes and olefin selectivities in the MTO reaction (with SAPOs, the Bronsted acid sites are typically isolated)[14]. The synthesis of small pore zeolites with cages and higher Si/Al typically involve the use of organic quaternary ammonium cations (Structure-Directing Agents, here denoted SDAs). The SDAs organize and nucleate zeolitic structures with cages of sufficient size to accommodate them, and the design of new SDAs opens opportunities for discovering new small pore, cage-containing zeolites. Additionally, it is possible to develop intergrowths between closely related zeolite structures and their behavior can be distinguished from the parent zeolite performances. Figure 1 shows a representation of such SDA structures residing in the pores of zeolites SSZ-13 (CHA) [15] and SSZ-39 (AEI) [16]. In the latter case, the SDA can have isomeric configurations, and one is preferred in the crystallization of the SSZ-39 [6, 17-19]. Thus, there is a rich chemistry for creating new zeolite structures via the use of SDAs, and a number of them will be described herein.

In this contribution, we extend both the types of different crystalline structures, including a number of newly discovered materials, and their compositions that are investigated as catalysts for the MTO reaction. We focus on the relationships between the structural features of these zeolite catalysts and their selectivities for light olefins and lifetimes of the reaction. Of particular interest are structures that significantly alter light olefin ratios from those observed from the commercial catalyst (SAPO-34).

EXPERIMENTAL

Syntheses of SAPO-34 and Zeolites

The SAPO-34 and zeolite samples used in this work were prepared from previously reported literature methods: SAPO-34 [3] (CHA), SSZ-13 [6] (CHA), SSZ-16 [20] (AFX), SSZ-52 [21] (SFW), SSZ-98 [22] (ERI), SSZ-105 [23], SSZ-99 [24], SSZ-104 [25], SSZ-27 [26], ITQ-3-type material (ITE) [27], and SSZ-28 [28] (DDR). Calcination was performed at 540-580 °C for 5-6 hours. For ion-exchange, typically, organic-

removed zeolites were dispersed in 1 M NH_4NO_3 solution with a solid-solution ratio of 1 g:100 ml, and this mixture was heated to 85-90 °C and stirred for 24 hours. After that, solid was recovered by filtration or centrifuge, and re-dispersed in fresh solution and heated up again. This procedure was repeated until no alkali metal is detected by energy dispersive spectroscopy (Oxford X-max SDD detector built in Zeiss 1550VP field emission scanning electron microscopy (FE-SEM)). The NH_4-form zeolites were completely dried in at 100 °C before catalysis evaluation.

Catalyst Characterizations

Powder X-ray diffraction (PXRD) profiles were obtained from all samples to determine framework topologies and phase purities using a Rigaku Miniflex II diffractometer using Cu Kα radiation.

Elemental compositions were determined via scanning electron microscopy/energy dispersive spectroscopy (SEM/EDS) on a ZEISS 1550VP instrument equipped with an Oxford X-Max SDD energy dispersive X-Ray spectrometer. Silicon to aluminum ratios were calculated from bulk elemental analyses.

Reaction Testing

The performances of the catalysts were tested at atmospheric pressure using a fixed-bed, stainless steel reactor of a dimension of 0.25" I.D. X 6" length. Typically, 200 mg of each dried catalyst sample was pelletized before being loaded between two plugs of glass wool. The granular size of pelletized catalyst was controlled to be 0.18-0.60 mm using a pair of ATSM meshes. Under a dry air flow, the temperature was increased to 150 °C and held for 3 hours. Next, the temperature was increased to 580 °C and held for 12 hours. The temperature ramping rate was controlled at 1 °C min^{-1} for all cases.

The weight-hourly space velocity (WHSV) of methanol with respect to the catalysts was controlled to be ~ 1.3 h^{-1}. The net methanol injection rate was typically 5.0-5.4 µl/min to achieve this WHSV, depending on the actual dried weight of catalyst loaded in the reactor. All reactions were performed at 400 °C under a 10% methanol/inert (95% He-5% Ar internal GC standard) flow of 30 ml min^{-1} volumetric flow rate. The gas phase flow over the catalyst was switched from the calcination air to the reaction gas flow after the stabilization of desired methanol level was achieved. The product identification and evaluation were conducted using an Agilent GC-MS system (GC: Agilent 6890N; MS: Agilent 5973N). Aliquots of product flow were taken and analyzed every 16 min. The amounts of hydrocarbon products formed over the catalysts were evaluated by calculating the selectivities from the resultant GC-chromatograms. All selectivity values in this work were calculated on the carbon-number basis.

RESULTS AND DISCUSSION

The objectives of our work are to prepare a number of small pore, cage-containing zeolites, and to test their behavior as catalysts for the MTO reaction in order to investigate: (i) whether zeolite

3

structure-reaction properties relationships can be ascertained, and (ii) whether light olefin selectivities can be altered by cage architectures. Table 1 summarizes the catalysts that are investigated here. (Schematic drawings of the cages are provided in the Supporting Information) Of particular interest to our study are any relationships between zeolites constructed with "double 6-ring" (D6R) features and their propensity to be effective MTO catalysts. For example, CHA and AEI both contain D6Rs as can be seen in Figure 1. This feature has received prominent attention in the analysis of effective deNO$_x$ catalysts, with the question being asked, " is the D6R an important site for the Al to be located for the copper exchange and subsequent function, and do these environments better promote the ability to have near neighbor pairs of Al sites that is the key contributor to effective catalysis? " In the deNO$_x$ research area, Gounder and co-workers have focused on controlling Al site populations via direct synthesis methods [29]. Acid site proximity has already been shown to influence the MTO behavior with completely isolated sites revealing behavior most similar to that observed from SAPO-34 [14]. Thus, these types of structural features are investigated here also by examining D6R-containing materials such as CHA and AFX (data previously reported from AEI [6] will also be used for comparisons) (vide infra), and expand the group with the addition of a newer member that has the largest cage in this collection, namely SSZ-52. A schematic of the SSZ-52 structure is shown in Figure 2. This zeolite is formed as a result of the cage-filling with two SDAs (not just a single bulky organo-cation) and the filling relationship is shown in Figure 2 [21].

Previously, Bhawe et al. [7] explored the relationship between the zeolite cage size and the MTO reaction behavior when the crystal sizes and Si/Al ratios were held relatively constant. Three D6R-containing zeolites where studied: CHA (SSZ-13), AFX (SSZ-16; larger cage than CHA) and LEV (SSZ-17: smaller cage than CHA). Here, we add to this suite of materials by including intergrowth materials of LEV and ERI (SSZ-105), and a high-silica ERI material (SSZ-98). Also, SSZ-99 that is an intergrowth of CHA and GME, is tested. We group all these materials together as they lack any pentasil construction component, and thus contain 4 and 6 ring sub-units. These materials are easier to synthesize with higher Al contents, and indeed CHA and ERI can be found as minerals with Si/Al = 2-3. We include also in our investigation materials where there are pentasil components; DDR, ITE and a previously unreported small pore zeolite, SSZ-27. This latter group of zeolites is difficult to prepare with Si/Al much below Si/Al = 14. Thus, we now also have higher Si/Al versions of the D6R zeolites (CHA, AEI [6], AFX) so we can make comparisons to the non-D6R zeolites. The crystallite sizes of the samples are all within the range of 0.5–30 μm. Since the crystallite sizes of MTO catalytic materials have been shown to mainly affect the catalytic lifetime, and have only a weak correlation with the light olefin product distributions [30]) (the primary focus of this work), crystallite size effects are not investigated here.

Figure 3 shows time-on-stream profile data for the conversion of methanol to the key products of interest. The reaction conditions used in this investigation are not optimized for any given material, but selected to provide conversions and lifetimes that provided the ability to compare a very broad spectrum of zeolites. While it is well known that reaction results vary with conditions, we did not vary the reaction conditions within this study. Zeolites illustrated in Figure 3 all contain D6Rs. SAPO-34 is included in Figure 3 for comparative purposes, and the results shown are in good agreement with the literature on this material. SAPO-34 gives high light olefin yields, ethylene/propylene ratios of ca. 1 and

long lifetimes. The aluminosilicate analogue of SAPO-34 is SSZ-13. Previously, reaction data from SAPO-34 has been compared to those obtained from SSZ-13 (initially, Yuen et al. [5], and subsequently many others). Here, the results are comparable to Yuen et al. and show that SSZ-13 with a Si/Al ca. 20 gives good C_2-C_4 olefin make, but with shorter lifetimes. Recently, it has been reported that higher Si/Al SSZ-13 can perform similar to SAPO-34 in the MTO reaction [14]. It was concluded from that study that higher Si/Al is necessary to create completely isolated acid sites in SSZ-13 (SAPO-34 has essentially isolated acid sites by the nature of the Si substitution mechanism) [14].

SSZ-16 (AFX) and SSZ-52 (SFW) have larger cages than SSZ-13. These materials, when they first come on stream, produce a large amount of propane and have shorter lifetimes. This also occurs with lower Si/Al SSZ-13's [14]. However, note that the behavior of higher Si/Al SSZ-16 is not improved as significantly as is observed when increasing the Si/Al of SSZ-13 [14]. In these larger cage materials, SSZ-16 and SSZ-52, there is a high production of propane that diminishes before there is a breakthrough of DME formation (related to catalyst deactivation). As propane is likely symptomatic of aromatic species formation, higher propane production has been be shown to correlate with shorter catalyst lifetimes presumably due to aromatics filling the cages of the zeolite to cause deactivation [14]. The data from SSZ-16 and SSZ-52 at Si/Al = 6 are quite similar (Figure 3). It is interesting that the product selectivity and deactivation profiles do not vary much as the cage size increases from SSZ-16 to SSZ-52; however, the cage sizes only increase in the c-direction as the cage diameter and pore sizes are essentially the same. Figure 3d shows reaction profile data for SSZ-16 having a higher Si/Al. Two interesting features emerge. First, the deactivation occurs at a later time, as the number of Al sites are reduced (compare the data shown in Fig. 3c to those in Fig. 3d). Second, the initial propane yield is not as high as is obtained in the more Al-rich SSZ-16 and the SSZ-52. These results are consistent with the trends observed with SSZ-13 [14]. However, they do not show such dramatic improvements that are seen with SSZ-13. Thus, cages larger than the CHA cage appear to more readily produce organic species that lead to faster deactivation.

Reaction data for the ERI-based materials, SSZ-98 and SSZ-105, are illustrated in Figure 4. These materials have a dimension of the cage size that is smaller than CHA. First, note that the propane make is not as high as observed from SSZ-16 and SSZ-52, even though the materials have similar Si/Al ratios. Second, there are time points in the reaction where the ethylene/propylene ratio is much higher than observed in the previous group of zeolite materials (and will also be the case relative to the pentasil type zeolites discussed below). The highest ethylene/propylene ratio is observed at times where there is deactivation starting to occur. It is interesting that when there is some LEV intergrowth (SSZ-105), there is still high ethylene selectivity. Previous studies from Bhawe et al. [7] on the LEV structure did show an enhanced ethylene/propylene ratio over the SSZ-13 and SSZ-16, but the ratio is not nearly as high as observed here for ERI. The ethylene/propylene ratio rises to an almost 3:1 ratio at some time points as the deactivation is beginning. Importantly, the overall olefins production remains high. Thus, there must be a key event occurring as the nature of the zeolite cage is being altered by components of the reaction. It would be useful to have an analysis of the reaction intermediates with time-on-stream [14], but that work is beyond the scope of this study.

As discussed above, reaction features of the ERI structure are manifested in intergrowth materials. Therefore, zeolites that are CHA, namely SSZ-99 (intergrowth with GME) and SSZ-104 were investigated. The MTO reaction results for SSZ-99 and SSZ-104 are shown in Figure 5. Unfortunately, these materials are prepared with low Si/Al, so comparisons to the best reaction data from CHA samples are not possible. However, the reaction data from SSZ-99 and SSZ-104 appear consistent with CHA and other D6R zeolites in that the ethylene/propylene ratio is ca. 1, and time-on-stream data do begin with high propane yields. At this time, little more can be conclusively said about the reaction results from these samples.

Figure 6 illustrates the structures of three zeolites tested here that have pentasil sub-unit constructions. The time-on-stream data for these materials are shown in Fig. 7. While the olefin selectivities from SSZ-27 and DDR are not remarkable, the ITE material produces almost a 2:1 ratio for propylene over ethylene. Additionally, all three materials do produce significant amounts of propane and do not have particularly long times for complete methanol conversion. The deactivation rates (e.g., where DME is being observed as product) are 110, 60 and 30 minutes for DDR, ITE and SSZ-27, respectively. The SSZ-27 is particularly interesting in that the micropore volume of this new structure is reasonable (0.20 cc/gm for nitrogen uptake), but the channel system is tortuous and hindered. This structural feature may play a role in the rapid deactivation.

The data presented in Fig.8 summarizes the initial propane selectivities obtained here and from others reported in the literature (used the same reaction conditions). Deimund et al. showed previously that the initial propane selectivities decreased from a series of SSZ-13 samples with increasing Si/Al, and correlated these reaction data to the number of paired acid sites (measured by Cu^{2+} exchange) [14]. Propane production has been speculated by others to be the result of aromatic condensation to form polycyclic aromatics (with release of propane) within the cages of the zeolite to cause deactivation. Deimund et al. showed that catalyst lifetimes did correlate with initial propane selectivities (higher the propane the shorter the lifetime) [14]. Here, we have extended these correlations to include several other zeolites. From the data illustrated in Fig. 8, it is clear that like SSZ-13, numerous other zeolites show decreasing initial propane selectivities with increasing Si/Al (more isolated acid sites). Additionally, there appears to be a relationship between the largest dimension of the zeolite cage and the initial propane selectivity. For a given Si/Al, the larger the dimension, the more propane (and decreased lifetime). The trends are AFX, SFW > AEI, RTH, LTA, RHO > CHA > LEV, ERI. These results show that high Si/Al and smaller cages lead to less initial propane and subsequently longer lifetimes.

Figure 9 shows the product selectivities from the zeolite materials investigated in this study as well as several other zeolites that have been reported in the literature (using the same reaction conditions). Analysis of these results reveals four types of behavior: (i) ethylene greater than propylene with low butene; SSZ-17, SSZ-98, SSZ-105, (ii) ethylene equal to propylene and low butene; SAPO-34, SSZ-13, SSZ-16, SSZ-27, SSZ-52, SSZ-99, SSZ-104, (iii) propylene greater than ethylene with butene similar to ethylene; SSZ-28, SSZ-39, SSZ-50, ITE and (iv) ethylene equal to propylene equal to butene; LTA, RHO. For higher ethylene yields, ERI- and LEV-based structures stand out. Other reports of LEV-based materials (zeolites [7, 34]) and ERI-based SAPOs (SAPO-17 [35]) also show ethylene/propylene ratios above unity at reaction temperature of 400 °C. Both of these structures have cages that are smaller than

the cage in CHA (SAPO-34, SSZ-13). ERI, LEV, CHA, AFX and SFW are members of the ABC-6 family of zeolites, where the largest dimension of the cage is determined by the ABC-6 stacking order. ERI and LEV have the smallest cage size dimension as well as the smallest pore dimensions. SSZ-52 (SFW) possesses the largest cage (Fig. 2). While the zeolites with the smallest cage size dimension do give the largest selectivities to ethylene, there are no other relationships that are consistent with all the data provided.

LTA and RHO give ethylene, propylene and butene selectivities that are about the same, e.g, near 1/1/1. Both of these structures contain the same large, spherical cage. It is interesting to note that while the series CHA, AFX, SFW have cages that increase in one dimension, there is not an increase in butene selectivity as the size expands. These data clearly show that it is not only size that is important to reaction selectivities but also shape.

What remains of high interest is how structures are able to form high propylene selectivities. For example, compare the results from CHA to those from AEI (Fig. 1). There is a dramatic shift in the selectivities for these two materials. At high Si/Al (and long, stable lifetimes like SAPO-34), CHA gives ca. ca. 40% ethylene, 40% propylene, 15% butene [14] while AEI yields ca. 56% propylene, 18% ethylene and 20% butene [6]. High propylene yields are also observed from the DDR topology, e.g., SSZ-28 here and other literature data [34, 36]. Thus, structural features such as D6R or pentasil arrangements appear not to be the dominate reason for high propylene selectivity.

While we are not able to find a unifying concept to explain the light olefin selectivity-zeolite structure relationship, we have now clearly identified four classes of behavior. Our results do provide leads for further investigations.

REFERENCES

[1] P. Tian, Y. Wei, M. Ye, Z. Liu, *ACS Catal.* 2015, *5*, 1922-1938.
[2] B.M. Lok, C.A. Messina, R.L. Patton, R.T. Gajek, T.R. Cannan, E.M. Flanigen, US Patent 4,440,871, 1984.
[3] G. Liu, P. Tian, J. Li, D. Zhang, F. Zhou, Z. Liu, *Micropor. Mesopor. Mater.* 2008, *111*, 143-149.
[4] L. Sierra de Saldarriaga, C. Saldarriaga, M.E. Davis, *J. Am. Chem. Soc.* 1987, *109*, 2686-2691.
[5] L.-T. Yuen, S.I. Zones, T.V. Harris, E.J. Gallegos, A. Auroux, *Micropor. Mater.* 1994, *2*, 105-117.
[6] M. Dusselier, M.A. Deimund, J.E. Schmidt, M.E. Davis, *ACS Catal.* 2015, *5*, 6078-6085.
[7] Y. Bhawe, M. Moliner-Marin, J.D. Lunn, Y. Liu, A. Malek, M. Davis, *ACS Catal.* 2012, *2*, 2490-2495.
[8] D.W. Fickel, R.F. Lobo, *J. Phys. Chem. C* 2010, *114*, 1633-1640.
[9] J.D. Albarracin-Caballero, I. Khurana, J.R. Di Iorio, A.J. Shih, J.E. Schmidt, M. Dusselier, M.E. Davis, A. Yezerets, J.T. Miller, F.H. Ribeiro, R. Gounder, *React. Chem. Eng.* 2017, *2*, 168-179.
[10] L. Ma, Y. Cheng, G. Cavataio, R.W. McCabe, L. Fu, J. Li, *Chem. Eng. J.* 2013, *225*, 323-330.
[11] M.A. Deimund, J.E. Schmidt, M.E. Davis, *Top. Catal.* 2015, *58*, 416-423.

[12] J. Chen, J. Li, Y. Wei, C. Yuan, B. Li, S. Xu, Y. Zhou, J. Wang, M. Zhang, Z. Liu, *Catal. Commun.* 2014, *46*, 36-40.

[13] J. Li, Y. Wei, J. Chen, S. Xu, P. Tian, X. Yang, B. Li, J. Wang, Z. Liu, *ACS Catal.* 2015, *5*, 661-665.

[14] M.A. Deimund, L. Harrison, J.D. Lunn, Y. Liu, A. Malek, R. Shayib, M.E. Davis, *ACS Catal.* 2016, *6*, 542-550.

[15] S.I. Zones, US Patent 4,544,538 A, 1985.

[16] S.I. Zones, Y. Nakagawa, S.T. Evans, G.S. Lee, US Patent 5,958,370 A, 1999.

[17] P. Wagner, Y. Nakagawa, G.S. Lee, M.E. Davis, S. Elomari, R.C. Medrud, S.I. Zones, *J. Am. Chem. Soc.* 2000, *122*, 263-273.

[18] M. Dusselier, J.E. Schmidt, R. Moulton, B. Haymore, M. Hellums, M.E. Davis, *Chem. Mater.* 2015, *27*, 2695-2702.

[19] R. Ransom, J. Coote, R. Moulton, F. Gao, D.F. Shantz, *Ind. Eng. Chem. Res.* 2017, *56*, 4350-4356.

[20] R.H. Archer, S.I. Zones, M.E. Davis, *Micropor. Mesopor. Mater.* 2010, *130*, 255-265.

[21] D. Xie, L.B. McCusker, C. Baerlocher, S.I. Zones, W. Wan, X. Zou, *J. Am. Chem. Soc.* 2013, *135*, 10519-10524.

[22] D. Xie, S.I. Zones, C.M. LEW, T.M. Davis, US Patent 9,416,017, 2016.

[23] D. Xie, US Patent 9,663,377, 2017.

[24] S.I. Zones, D. Xie, C.Y. Chen, A.J.B. Liang, US Patent 9,193,600 B1, 2015.

[25] T.M. Davis, US Patent 9,725,328 B1, 2017.

[26] S.I. Zones, D. Xie, R.J. Saxton, US Patent 9,505,627 B1, 2016.

[27] G.S. Lee, S.I. Zones, Y. Nakagawa, S.T. Evans, US Patent 6,218,591 B1.

[28] S.I. Zones, D.L. Holtermann, R.A. Innes, US Patent 5,200,377 A, 1993.

[29] J.R. Di Iorio, R. Gounder, *Chem. Mater.* 2016, *28*, 2236-2247.

[30] N. Nishiyama, M. Kawaguchi, Y. Hirota, D. Van Vu, Y. Egashira, K. Ueyama, *Appl. Catal. A* 2009, *362*, 193-199.

[31] J.E. Schmidt, M.A. Deimund, D. Xie, M.E. Davis, *Chem. Mater.* 2015, *27*, 3756-3762.

[32] B.W. Boal, J.E. Schmidt, M.A. Deimund, M.W. Deem, L.M. Henling, S.K. Brand, S.I. Zones, M.E. Davis, *Chem. Mater.* 2015, *27*, 7774-7779.

[33] Y. Ji, J. Birmingham, M.A. Deimund, S.K. Brand, M.E. Davis, *Micropor. Mesopor. Mater.* 2016, *232*, 126-137.

[34] J. Goetze, F. Meirer, I. Yarulina, J. Gascon, F. Kapteijn, J. Ruiz-Martínez, B.M. Weckhuysen, *ACS Catal.* 2017, *7*, 4033-4046.

[35] S. Nawaz, S. Kolboe, M. Stöcker, Conversion of Methanol to Light Olefins over Sapo-17 Molecular Sieve, in: H.E. Curry-Hyde, R.F. Howe (Eds.) Stud. Surf. Sci. Catal., Elsevier, 1994, pp. 393-398.

[36] Y. Kumita, J. Gascon, E. Stavitski, J.A. Moulijn, F. Kapteijn, *Appl. Catal. A* 2011, *391*, 234-243

Table 1. Catalysts investigated, their topological information, their Si/Al ratios and reaction lifetimes.

	Topological Information				Sample/Catalytic Information		
Material	Framework	Channel dimensionality	Maximum size of sphere able to be included (Å)	Cage Dimensions* (Å)	Si/Al†	Time to 80% MeOH Conversion (min)	Time to 1% DME Formation (min)
SAPO-34	CHA	3D	7.37	$8.33 \times 7.45 \times 7.05$	-	>200	93
SSZ-13	CHA	3D	7.37	$8.33 \times 7.45 \times 7.05$	21.8	210	156
SSZ-16	AFX	3D	7.76	$13.13 \times 7.44 \times 7.05$	6.2	169	55
SSZ-16	AFX	3D	7.76	$13.13 \times 7.44 \times 7.05$	14.7	>200	73
SSZ-52	SFW	3D	7.78	$18.07 \times 7.45 \times 7.02$	6.1	112	53
SSZ-98	ERI	3D	7.04	$12.48 \times 6.76 \times 6.73$	5.7	117	85
SSZ-105	ERI/LEV	3D/2D	7.10 (LEV) 7.04 (ERI)	$7.15 \times 6.84 \times 6.59$ (LEV) $12.48 \times 6.76 \times 6.73$ (ERI)	9.3	245	71
SSZ-99	CHA/GME	3D	7.37 (CHA)	$8.33 \times 7.45 \times 7.05$ (CHA)	3.7	79	51
SSZ-104	CHA-related ABC-6 stacking fault	3D	7.37 (CHA)	$8.33 \times 7.45 \times 7.05$ (CHA)	3.6	44	25
SSZ-27	-	1D	7.15	$13.84 \times 7.18 \times 6.75$	14.8	43	14
ITQ-3-type	ITE	2D	8.30	$11.06 \times 10.34 \times 7.10$	18.1	90	73
SSZ-28	DDR	2D	7.66	$9.29 \times 7.07 \times 6.73$	18.8	312	105

* Cage dimensions were estimated based on an assumption that the framework atoms are hard spheres of diameters of 2.7 Å.

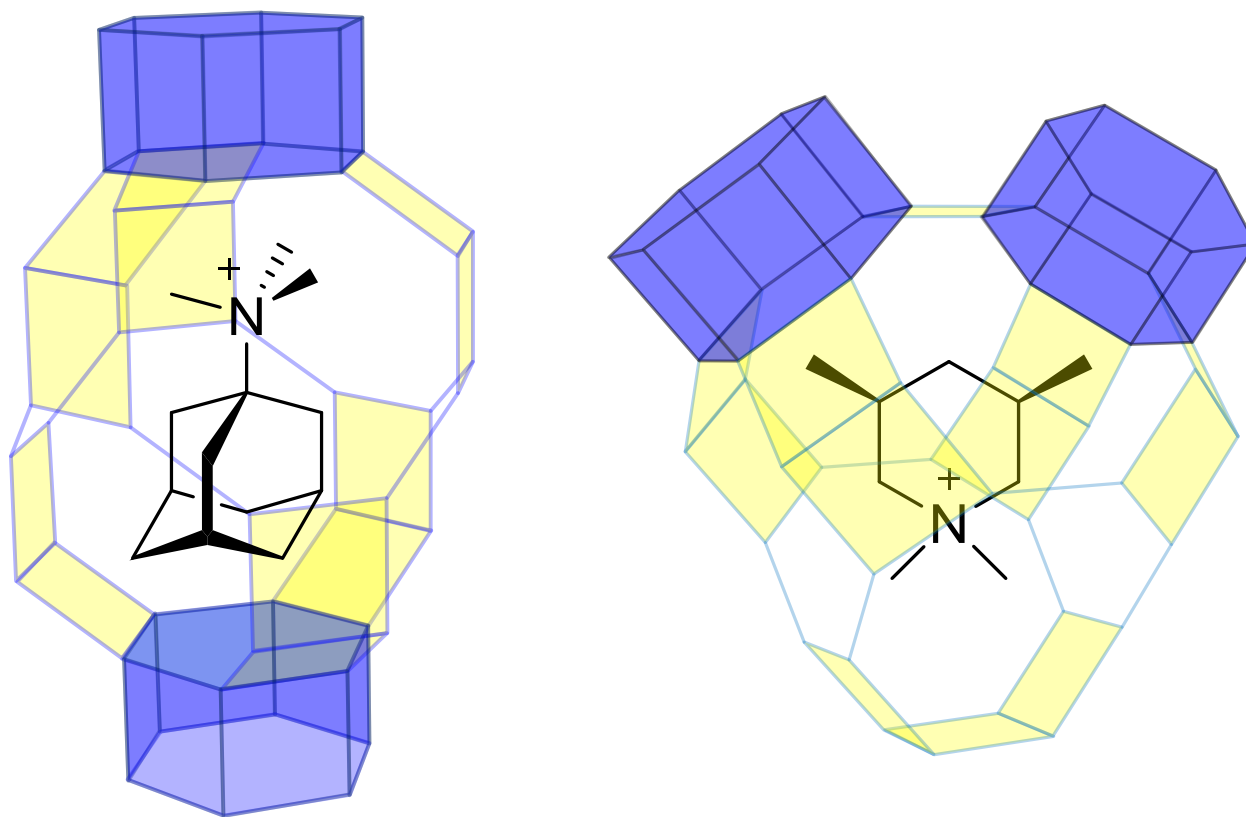† Si/Al ratios were characterized using EDS.

9

Figure 1. Schematic illustrations of the cage structures of CHA (left) and AEI (right) with their SDA molecules. $D6R$ building units are highlighted in blue color.
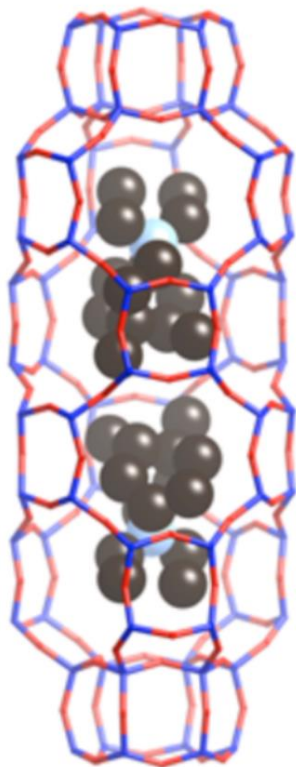
Figure 2. Schematic illustration of the large cavity of SSZ-52 that contains two SDA molecules. (Adapted from [21]).
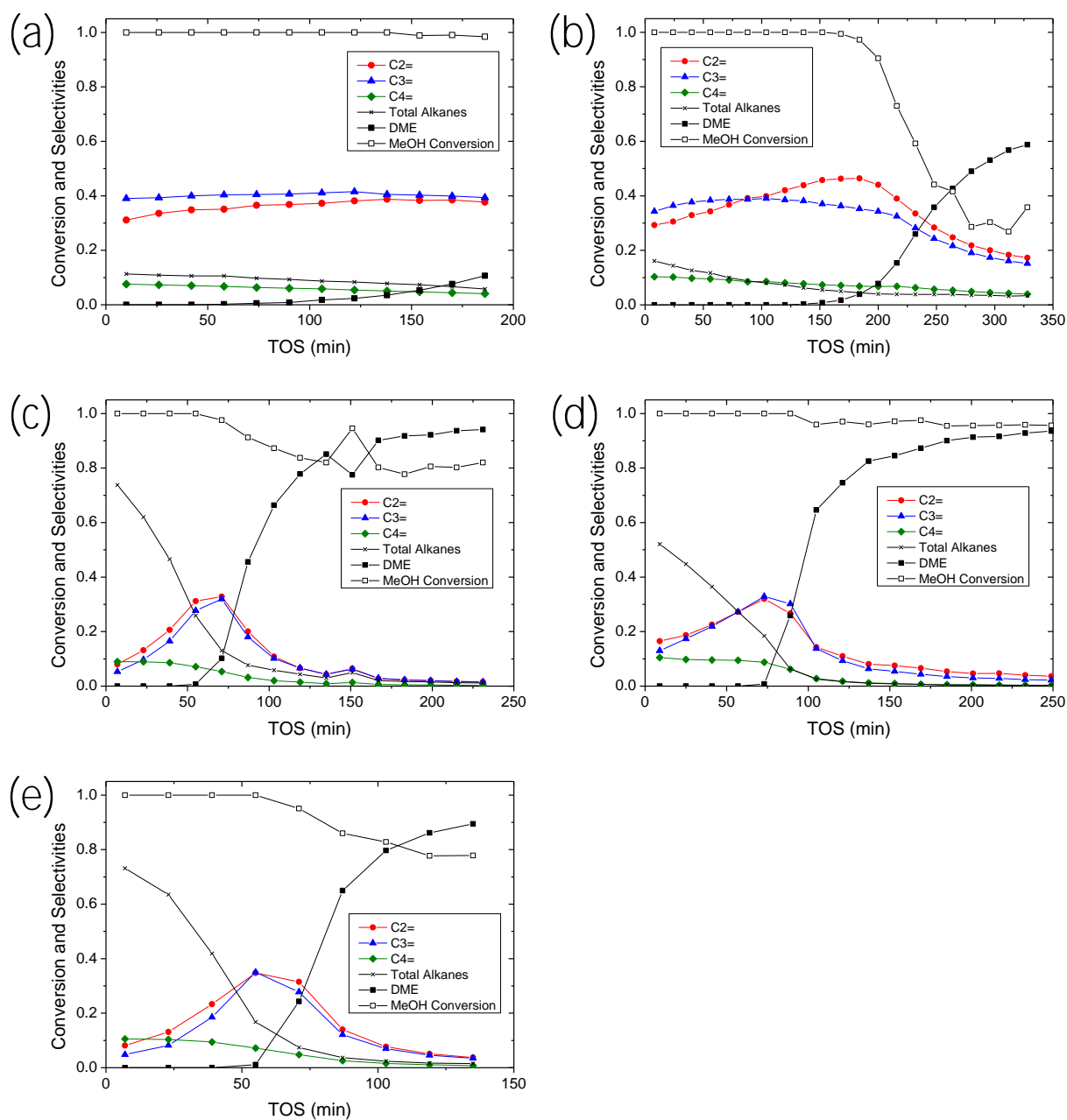
11

Figure 3. MTO-reaction time-on-stream (TOS) profiles acquired at 400 °C for: (a) SAPO-34, (b) SSZ-13 (Si/Al = 21.8), (c) SSZ-16 (Si/Al = 6.2), (d) high-silica SSZ-16 (Si/Al = 14.7), and (e) SSZ-52 (Si/Al = 6.1). Data listed as total alkanes primarily propane.
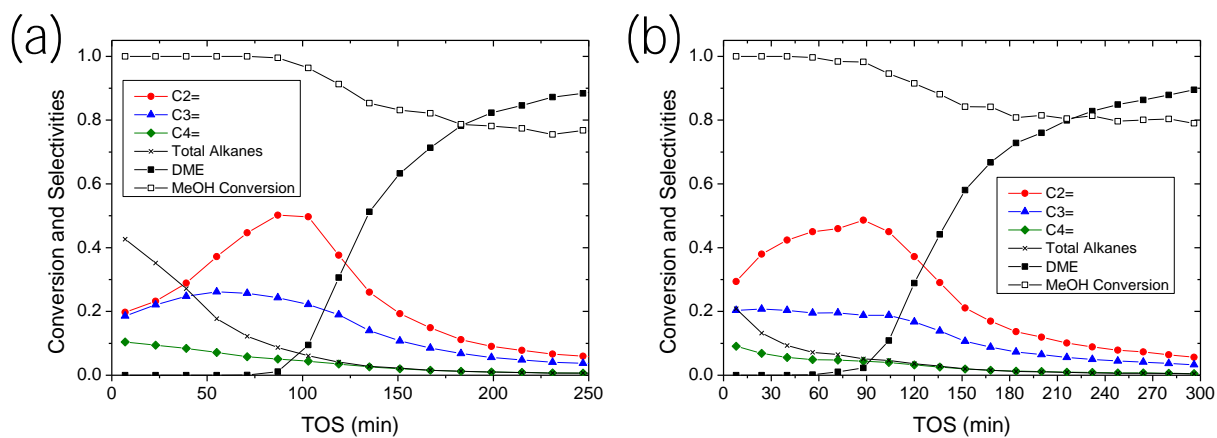
Figure 4. MTO-reaction time-on-stream (TOS) profiles acquired at 400 °C for: (a) SSZ-98 (Si/Al = 5.7), and (b) SSZ-105 (Si/Al = 9.3).
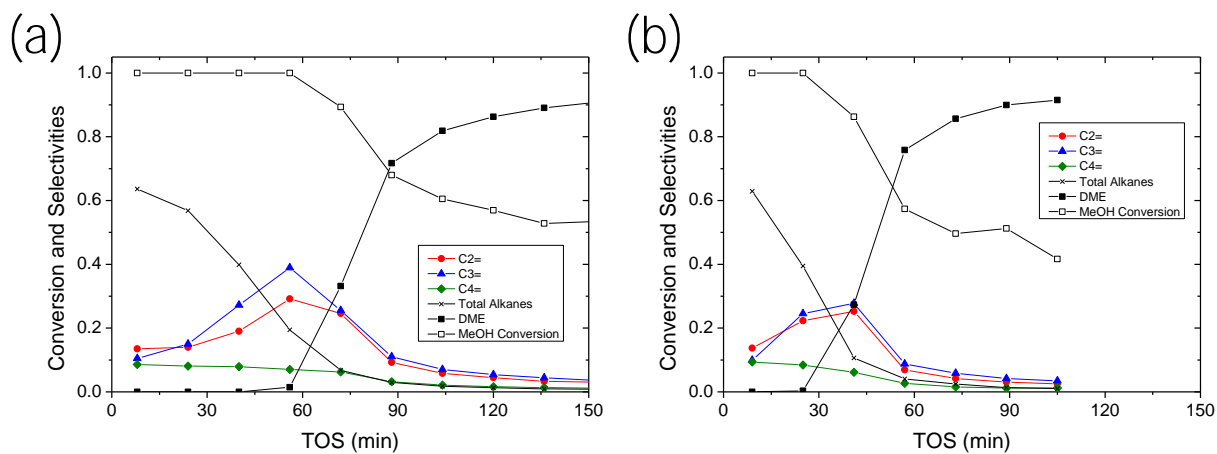
Figure 5. MTO-reaction time-on-stream (TOS) profiles acquired at 400 °C for: (a) SSZ-99 (Si/Al = 3.7), and (b) SSZ-104 (Si/Al = 3.6).

13
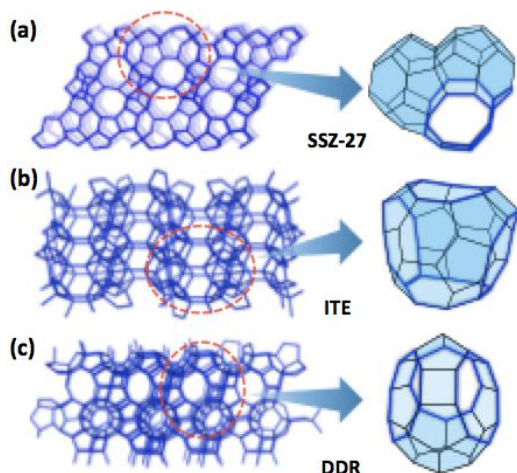
Figure 6. Schematic illustrations of framework structures and cage architectures of: (a) SSZ-27, (B) ITE, and (c) DDR.
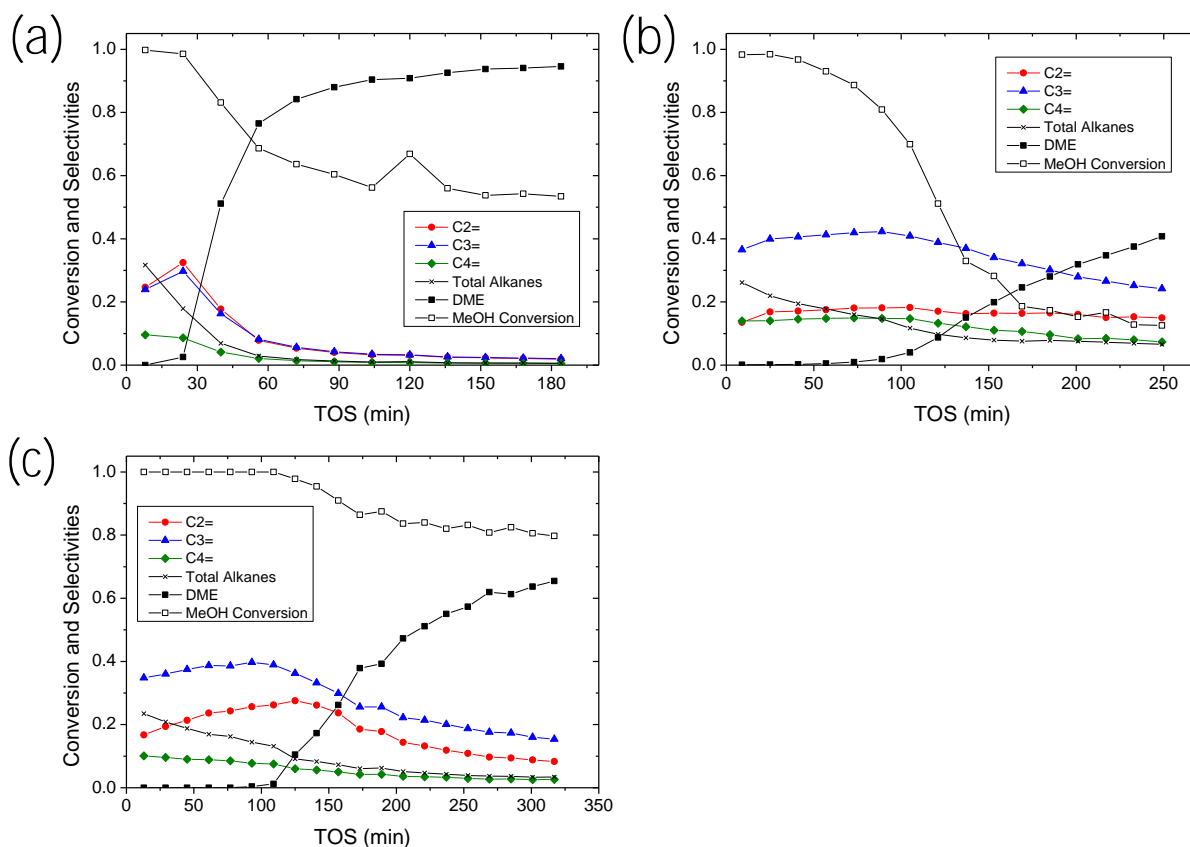

Figure 7. MTO-reaction time-on-stream (TOS) profiles acquired at 400 °C for: (a) SSZ-27 (Si/Al = 14.8), (b) ITE (Si/Al = 18.1), and (C) SSZ-28 (Si/Al = 18.8).
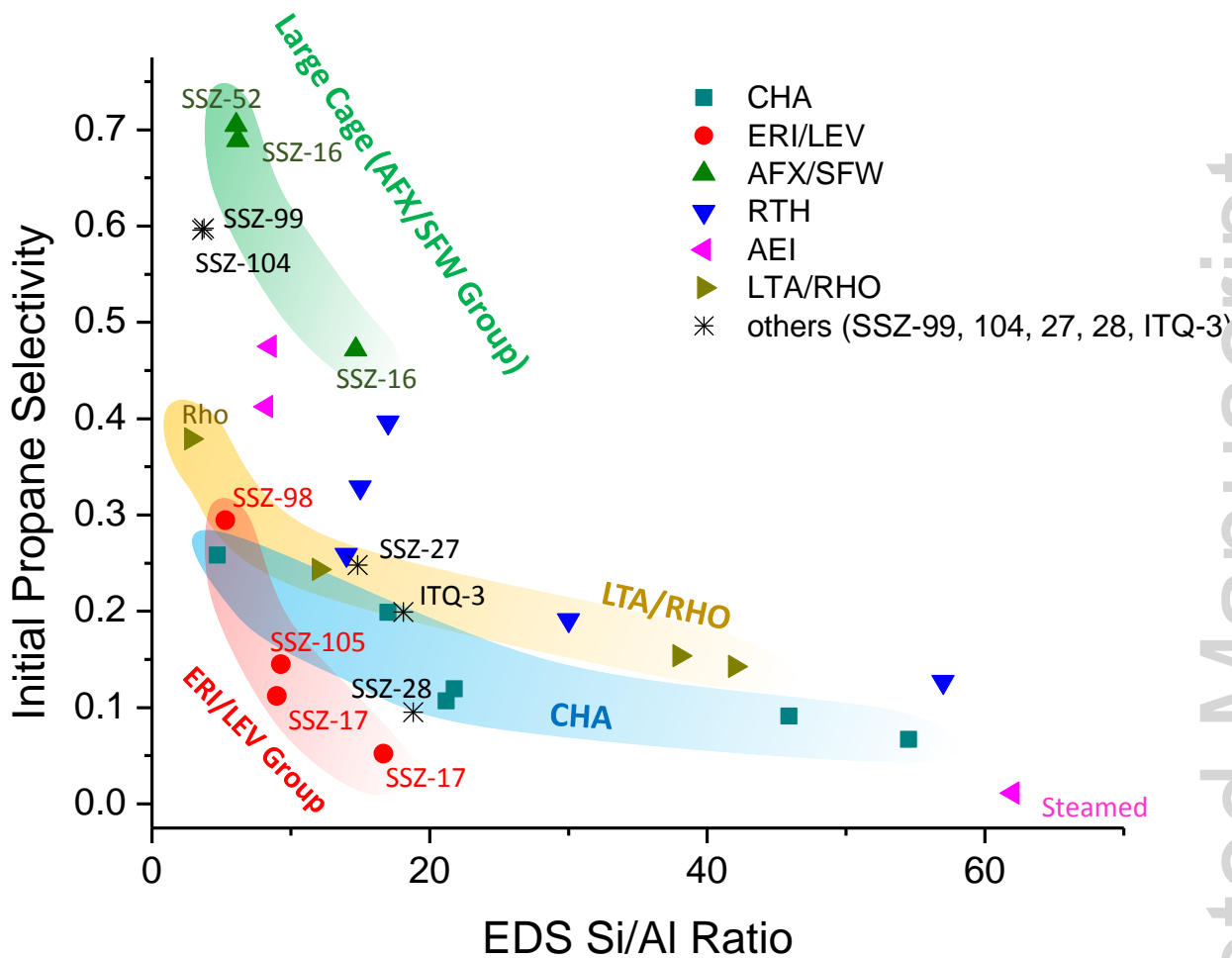
14

Figure 8. Initial propane selectivities (time-on-stream = 7-10 min) as a function of tetrahedral Si/Al for zeolite catalysts. The initial propane data points for SSZ-17 [7], RTH [31], LTA [32], Rho [33], SSZ-13 [14], and SSZ-39 [6] are from previous literature reports at the same reaction conditions.
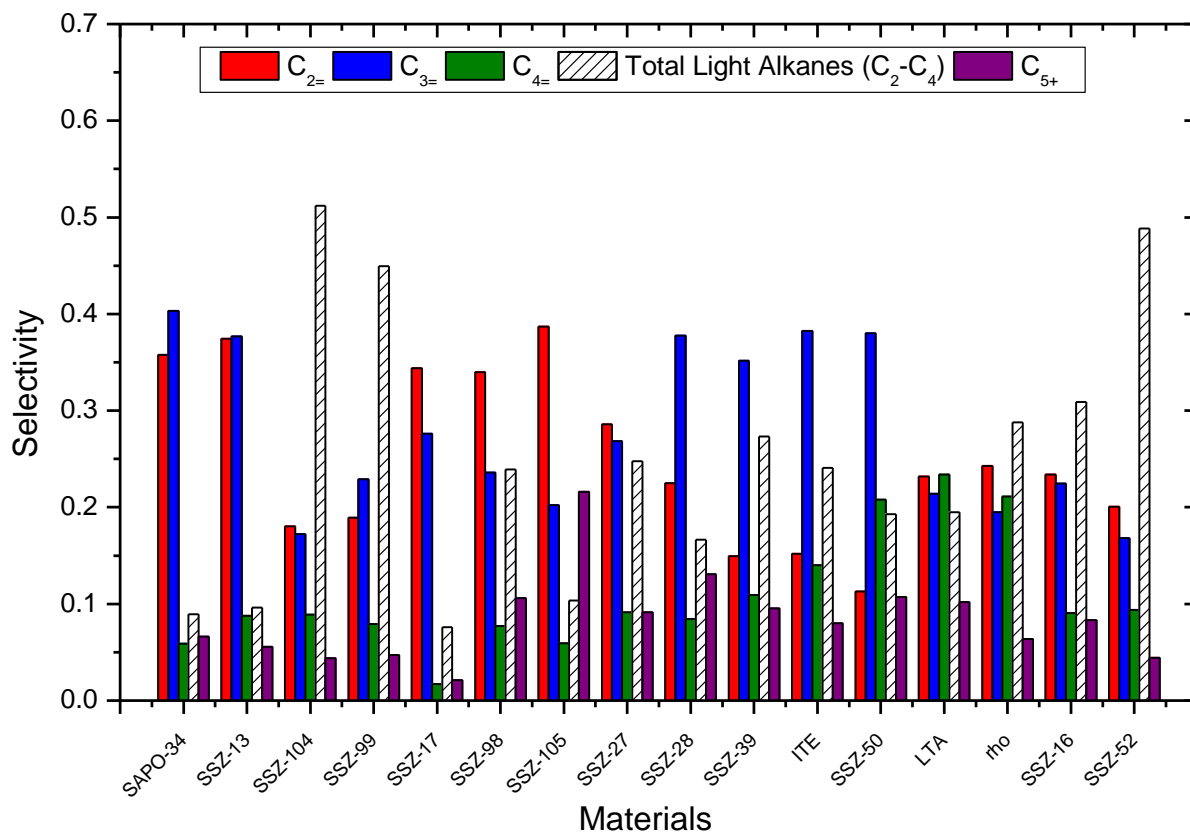
Figure 9. Product selectivities of zeolite catalysts compared to SAPO-34. The selectivity values are obtained by averaging hydrocarbon selectivities for conversions of methanol in the range of 98-100%. Selectivity data of SSZ-17 [7] (LEV), SSZ-39 [6] (AEI), SSZ-50 [31] (RTH), LTA [32], and Rho [33] are from previous literature reports at the same reaction conditions.

16

Table of Contents
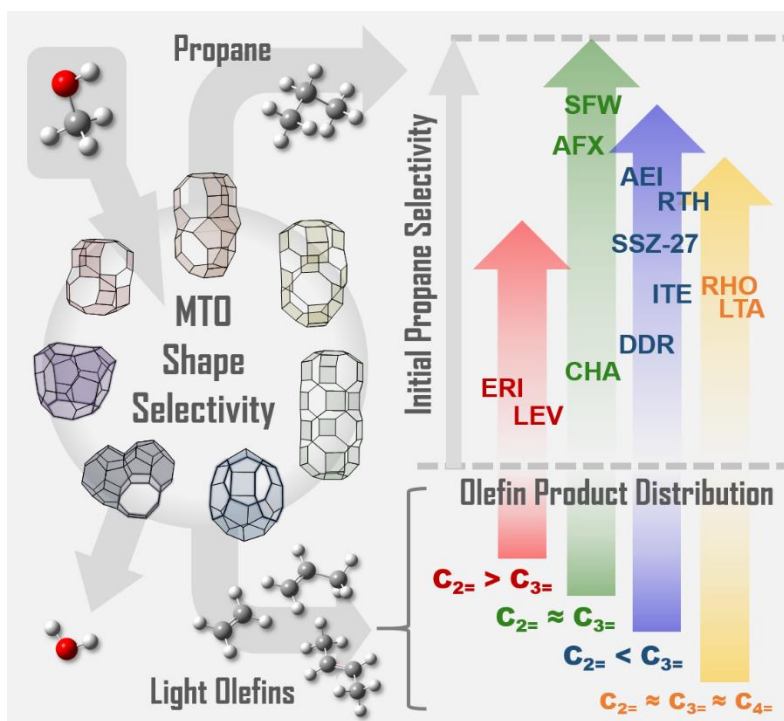
The structure-performance relationships in the methanol-to-olefin (MTO) reaction between the cage structures of small-pore molecular sieves and their resultant product distributions are investigated. Small-pore zeotypes of seven different topologies (CHA, ERI, AFX, SFW, DDR, ITE, and a new framework SSZ-27) are tested, and taken together with previously reported results, reveal four distinct trends in light olefin selectivity ratios. Additionally, the propane selectivity is found to depend not only the Si/Al ratios but also the dimensions of cages.

17